ARTICLE

Corrosion-resistant fluoridated Ca–Mg–P composite coating on magnesium alloys prepared via hydrothermal assisted sol–gel process

Yangyang Jiang[d]
Key Laboratory for Advanced Ceramics and Machining Technology of Ministry of Education, Tianjin University, Tianjin 300072, People's Republic of China

Lingjun Zhu[d]
Department of Orthopedic Surgery, Changzheng Hospital, Second Military Medical University, Shanghai 200003, People's Republic of China

Shu Cai[a]
Key Laboratory for Advanced Ceramics and Machining Technology of Ministry of Education, Tianjin University, Tianjin 300072, People's Republic of China

Sibo Shen[b]
Center for Electron Microscopy, Institute for New Energy Materials & Low-Carbon Technologies, School of Materials Science and Engineering, Tianjin University of Technology, Tianjin 300384, People's Republic of China

Yue Li, Song Jiang, Yishu Lin, Shaoshuai Hua, and Rui Ling
Key Laboratory for Advanced Ceramics and Machining Technology of Ministry of Education, Tianjin University, Tianjin 300072, People's Republic of China

Guohua Xu[c]
Department of Orthopedic Surgery, Changzheng Hospital, Second Military Medical University, Shanghai 200003, People's Republic of China

In this work, corrosion-resistant fluoridated Ca–Mg–P composite coatings were prepared on magnesium alloys via a hydrothermal assisted sol–gel process. All these coatings derived from Coating Sols with different F^- concentrations are composed of fluoridated hydroxyapatite, magnesium hydroxide, and dittmarite. When F^- concentration of Coating Sol is 0.03 M, the coating exhibited uniform and dense surface, and its thickness reached 32 μm, thus possessing a high charge transfer resistance of 312 ± 12.69 kΩ cm^2 in simulated body fluid (SBF). Immersion test in SBF showed that this coating could quickly induce the formation of the mineralized layer, implying relatively high bioactivity. After 49 days of immersion, the original composite coating and newly formed mineralized layer reached 60 μm in thickness, providing effective long-term protection for magnesium alloys. These attractive results indicate that this fluoridated Ca–Mg–P composite coating is a promising protective coating on biodegradable magnesium and magnesium alloy implants for orthopaedic applications.

I. INTRODUCTION

Magnesium and magnesium alloys are getting increasing attention as promising biodegradable metallic implants for orthopaedic applications, resulting from their excellent biocompatibility, low density, and high specific strength.[1,2] However, their poor corrosion resistance nature limits large-scale clinical application because of lacking long-term mechanical support for bone remolding and over alkalization of the surrounding physiological environment.[3,4] The desire to improve the corrosion resistance drives various development strategies, e.g., magnesium structural optimization, magnesium matrix composite with bioactive inorganic components, and coating modification.[5,6] Among them, employing biocompatible corrosion-resistant coatings is facile and effective.[7] Simultaneously, the biological properties of substrates could be modified via coating structural design.

Mainly, corrosion-resistant coatings should fulfill the application requirements in the physiological environment. Since single-component coatings commonly encounter more or less performance deficiency, designing composite coatings with the combined advantages of each component is an appealing strategy.[8] Generally, coating components should be selected on the basis of specific application requirements. $Mg(OH)_2$ is one of the most widely used corrosion-resistant coatings for magnesium and magnesium alloys due to its biocompatibility and nontoxic.

However, $Mg(OH)_2$ could be transformed into soluble $MgCl_2$ and gradually lose its protective effect.[9] So in multilayer coating structure, $Mg(OH)_2$ sometimes acts as the bottom layer to provide short-term protection until the surface layer protective coating formation. Furthermore, as one of the corrosion products of magnesium and magnesium alloys, $Mg(OH)_2$ could hinder their degradation to some extent.[10] Tang et al.[11] developed a thick $Mg(OH)_2$ coating on magnesium with a high bonding strength of 60 MPa. In addition to $Mg(OH)_2$, another magnesium-containing compound, i.e., dittmarite ($NH_4MgPO_4 \cdot H_2O$), possesses low solubility in aqueous environment and presents high chemical stability.[12] Zhao et al.[13] prepared a thick dittmarite/$Mg(OH)_2$ composite coating by hydrothermal method and the coating met biomaterial cytotoxicity standard. Ishizaki et al.[14] prepared a multilayered dittmarite/$Mg(OH)_2$ composite coating on magnesium alloys with excellent corrosion resistance. Nevertheless, bioactivity and mineralized capacity of the above composite coatings are somewhat unsatisfactory and require further improvement. Hydroxyapatite (HA), with chemical and structural similarity to human bone, possesses excellent biocompatibility and bioactivity.[15–17] Furthermore, bringing F^- into the HA lattice to form fluoridated hydroxyapatite (FHA) could make its structure compact and improve its bioactivity.[18] Wang et al.[19] prepared an FHA coating on magnesium alloys with favorable biocompatibility and osteoblastic cell response. In addition, FHA has lower solubility compared with HA.[20] Thus, it is reasonable to speculate that employing a kind of composite coatings, which is composed of $Mg(OH)_2$, $NH_4MgPO_4 \cdot H_2O$, and FHA, would endow magnesium alloys with favorable corrosion resistance and bioactivity.

To date, there are many methods available to prepare composite coatings, such as chemical conversion,[21] sol–gel,[22] microwave,[15] hydrothermal method,[13] etc. Generally, sol–gel method is environment-friendly, low-cost, and user-friendly.[23] Typically, the sol–gel process combined with hydrothermal method, i.e., two-step hydrothermal assisted sol–gel process, has been used to synthesize coatings or particles with well-defined crystallinity and morphology.[24–26] However, the one-step hydrothermal-assisted sol–gel process has seldom been reported. Herein, a new kind of fluoridated Ca–Mg–P composite coatings composed of FHA, $Mg(OH)_2$, and $NH_4MgPO_4 \cdot H_2O$ was prepared on magnesium alloys via the one-step hydrothermal assisted sol–gel process. In addition, the effects of fluorine doping on the coating composition, structure, and corrosion resistance performance were investigated.

II. MATERIALS AND METHODS

A. Magnesium alloy pretreatment

Commercial AZ31 magnesium alloy sheets were used as the substrates in the size of $10 \times 10 \times 2$ mm. First, the substrates were mechanically ground with SiC waterproof abrasive papers (#800, #1500, and #2000). Then, the substrates were immersed in NaOH solution (0.15 M) at 80 °C for 1 h, rinsed with deionized water and dried at 37 °C.

B. Coating preparation

First, 2.362 g $Ca(NO_3)_2 \cdot 4H_2O$ and 0.770 g $NH_4H_2PO_4$ were dissolved in 20 mL deionized water, respectively, and stirred for 30 min; 0.020 g, 0.040 g, and 0.060 g. NH_4F were dissolved in 10 mL deionized water, respectively, and stirred for 30 min. Then, three kinds of NH_4F solutions were added slowly into $NH_4H_2PO_4$ solutions and stirred for 30 min (Solution Is). Solution Is were added into $Ca(NO_3)_2$ solution with 30 min stirring (Solution IIs). Next, $NH_3 \cdot H_2O$ was added dropwise into Solution IIs to adjust the pH value to 10.0, stirring for 2 h, and left to settle for 12 h at room temperature to get Coating Sols. It is noted that Ca/P molar ratios of the as-received Coating Sols were 1.52 and F^- concentration of those were designed to be 0.01 M, 0.02 M, and 0.03 M, respectively. Finally, 25 mL Coating Sols with different F^- concentrations were put into stainless autoclave reactors with three pretreated magnesium alloy substrates, respectively, followed by hydrothermal treatment at 140 °C for 6 h. Then the samples were washed with deionized water and dried at 60 °C.[27] Coatings prepared from Coating Sols with different F^- concentrations (0.01 M, 0.02 M, and 0.03 M) were denoted as F1, F2, and F3, respectively.

C. Coating characterization

X-ray diffraction (XRD) was utilized to quantitatively calculate the phase contents of the obtained coatings. First, the coatings were scratched from the substrates for XRD pattern collection. Then, pattern fitting and quantitative measurement were conducted via MDI Jade 6.[28] JCPDS cards for $Mg(OH)_2$, $NH_4MgPO_4 \cdot H_2O$, and FHA were indexed as No. 44-1482, No. 36-1491, and No. 73-0293, respectively. The corresponding RIR values are 2.80, 3.42, and 1.07, respectively. Surface and cross-sectional morphology of the prepared coatings were examined by field emission scanning electron microscopy (SEM; S4800, Hitachi, Tokyo, Japan).

D. Electrochemical measurements

A typical three-electrode cell attached with an electrochemical workstation (CHI660C, Shanghai Chenhua instrument Co., Shanghai, China) was used to examine the electrochemical properties of the samples. Electrochemical impedance spectra (EIS) and potentiodynamic polarization measurements were conducted in simulated body fluid (SBF) at 37 °C. Five parallel assays were conducted to ensure repeatability.

E. Immersion tests

The in vitro immersion test was conducted in SBF at 37 °C using an incubator. SBF was updated every 2 days. After immersion for different times, the pH value of SBF and the corrosion rate of the samples were measured. In parallel, surface and cross-section morphology and electrochemical properties of the samples were analyzed. For detailed calculation methods, refer to our previous work.[15]

III. RESULTS AND DISCUSSION

A. Effects of fluorine doping on coating composition and structure

As is widely recognized, the performance of protective coatings greatly depends on their composition and structure.[29] Figure 1 shows XRD patterns of the obtained coatings prepared from Coating Sols with different F^- concentrations. Diffraction peaks of HA (JCPDS No. 73-0293), $Mg(OH)_2$ (JCPDS No. 44-1482), and $NH_4MgPO_4 \cdot H_2O$ (JCPDS No. 36-1491) were detected for F1, F2, and F3, meaning that all coatings are composed of FHA, $Mg(OH)_2$, and $NH_4MgPO_4 \cdot H_2O$. Phase contents of these composite coatings were calculated and are shown in Table I. With the increasing F^- concentration of Coating Sols from 0.01 to 0.03 M, FHA content in the composite coatings gradually decreases from approximately 68.3 wt% to approximately 62.8 wt%. In parallel, $Mg(OH)_2$ content gradually increases from approximately 29.9 wt% to approximately 36.7 wt%. Jiang et al. concluded that before FHA formation on the magnesium alloy, there existed reactions including the formation and solution of MgF_2, which happened only at a temperature above 90 °C.[17] However, in the reactor area of no magnesium alloy, some FHA crystals are prone to nucleate from Coating Sols. So it is reasonable to speculate that the calcium content of Coating Sols to form FHA on the magnesium alloy would gradually decrease with F^- concentration increasing from 0.01 to 0.03 M; thus F3 has the lowest FHA content of approximately 62.8 wt%. Moreover, with the solution of MgF_2, $Mg(OH)_2$ would start to form on the magnesium alloy.[30] With F^- concentration increasing from 0.01 to 0.03 M, MgF_2 content would increase so that the $Mg(OH)_2$ content within the composite coatings increased. So F3 has the highest $Mg(OH)_2$ content of approximately 36.7 wt%.

The surface morphology of the composite coatings is shown in Fig. 2. Remarkably, all these coatings exhibit integrated surface. Moreover, F3 is denser than F1 and F2. From the enlarged views [Figs. 2(b), 2(d), and 2(f)], all these coatings are composed of stick-like and plate-like crystals. Notably, there are many granules precipitating on the surface of F3, which might be related to the
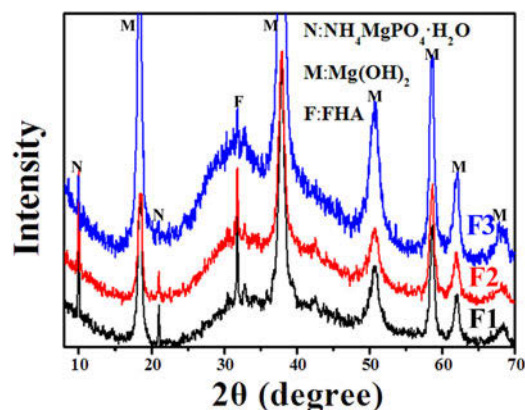

FIG. 1. XRD patterns of the obtained coatings: F1, F2, and F3.

TABLE I. Phase contents (wt%) of F1, F2, and F3.

Samples	FHA	$Mg(OH)_2$	$NH_4MgPO_4 \cdot H_2O$
F1	68.30 ± 6.12	29.90 ± 1.43	1.80 ± 0.05
F2	67.90 ± 10.00	30.10 ± 2.02	1.90 ± 0.07
F3	62.80 ± 17.58	36.70 ± 5.87	0.50 ± 0.01

increased content of $Mg(OH)_2$ within the composite coatings. These microrough coating surfaces might promote mineralized layer formation and osteogenic cell adhesion.[31]

Based on the above results, addition of fluorine into Coating Sols adjusted coating composition and structure. Especially, F3 with approximately 62.8 wt% FHA, approximately 36.7 wt% $Mg(OH)_2$, and approximately 0.5 wt% $NH_4MgPO_4 \cdot H_2O$ presented a uniform and dense surface. It is inferred that $Mg(OH)_2$ acted as the matrix for the composite coatings; dissolution-resistant FHA and $NH_4MgPO_4 \cdot H_2O$ crystals were embedded into the $Mg(OH)_2$ matrix to impose a strengthening effect. Thus effective protection of the composite coatings for magnesium alloys is expected.

B. Effect of fluorine doping on electrochemical properties of samples

Electrochemical tests, especially EIS and Tafel polarization measurements have proved efficient in assessing the corrosion resistance of the applied coatings. E_{corr} values and I_{corr} values of F1, F2, and F3 derived from the polarization curves [Fig. 3(a)] are presented in Table S1. High corrosion potential and low corrosion current density mean that a sample has low corrosion rate.[32] With the increasing fluorine doping content, E_{corr} shifted from approximately -1.42 V_{SCE} to approximately -0.80 V_{SCE}. According to the Tafel region, it was noted that I_{corr} changed oppositely. Among three samples, F3 presents the highest E_{corr} of approximately -0.80 V_{SCE} and lowest
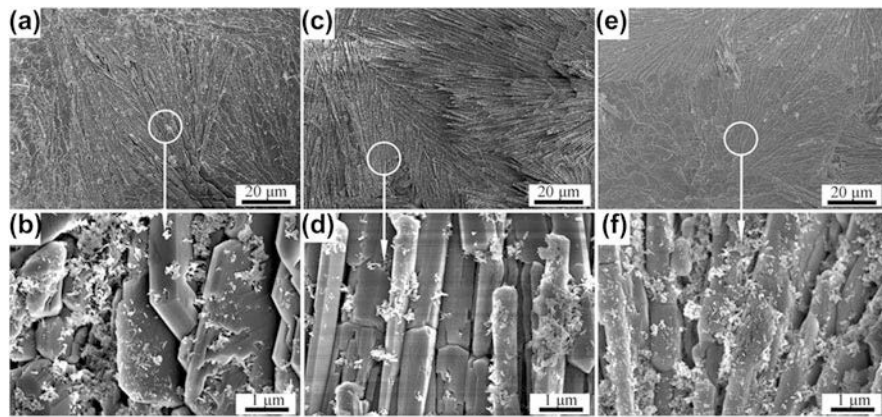
FIG. 2. Surface morphologies of the composite coatings: (a) F1, (c) F2, and (e) F3. The corresponding enlarged images of the composite coatings: (b) F1, (d) F2, and (f) F3.
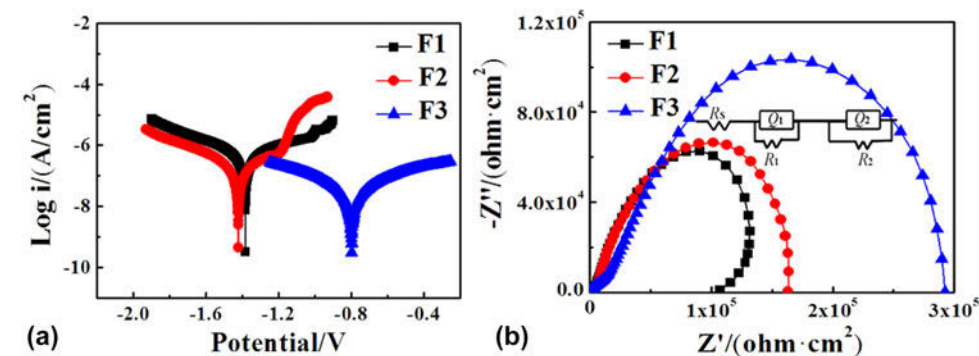

FIG. 3. (a) Tafel polarization curves and (b) Nyquist plots and the equivalent circuit for F1, F2, and F3 measured in SBF.

I_{corr} of approximately 0.02 μA/cm^2. In addition, the break potential, i.e., a sharp increase in current density with a small step in potential,[33] is discovered in the polarization curves of F1 and F2 except for F3, suggesting that F3 is more stable in SBF.

Moreover, Nyquist plots and Bode & phase plots of the samples are shown in Fig. 3(b) and Fig. S1. Capacitive loops of Nyquist plots with different shapes and diameters reflect impedance information.[34] Among three samples, similar equivalent circuits were applied to fit the Nyquist plots and the numerical fitting of EIS data is listed in Table II. R_s is the solution resistance; R_1 and Q_1 represent the resistance and capacity of the composite coating, respectively; R_1 and Q_1 characterize the capacitance performance and resistance property of the barrier Mg(OH)$_2$ layer, respectively. With the increase of fluorine doping content from F1 to F3, R_1 rose from approximately 165 to approximately 312 kΩ cm^2. F3 exhibited the highest impedance of approximately 312 kΩ cm^2, higher than the typical values of FHA and Mg(OH)$_2$ in the reported work (impedance of FHA was in the range from 1 to 10 kΩ cm^2 and that of Mg(OH)$_2$ was 10 kΩ cm^2).[11,15,22] Moreover, the phase angle of F3 remained a low and stable level at −40° compared with

that of F1 and F2, stating that F3 improved the impedance to a large degree.[35]

Combining the above XRD and SEM with electrochemical results, high corrosion resistance of F3 is mainly ascribed to the uniform and dense surface. So F3 is selected for further SBF immersion test.

C. Long-term protective effects of fluoridated Ca–Mg–P composite coating

To assess the long-time protective effect of the fluoridated Ca–Mg–P composite coating, immersion test in SBF was performed for F3. The immersion data of the naked magnesium alloy was reported in our previous work.[15] It is well-known that both coating dissolution and magnesium alloy degradation could cause SBF pH value variation. The pH value of a normal SBF should remain approximately 7.4. As shown in Fig. 4(a), the pH value of SBF immersing F3 gently changed in the range from 7.3 to 7.6 during immersion time to 49 days. However, the pH value of SBF immersing the naked magnesium alloy soared in the initial 4 days, and then kept stable at 10.4. Meanwhile, after immersion for 7, 14, 21, and 49 days, F3 was picked up to calculate the corrosion rate

TABLE II. Numerical fitting data of the Nyquist plots in Fig. 3(b).

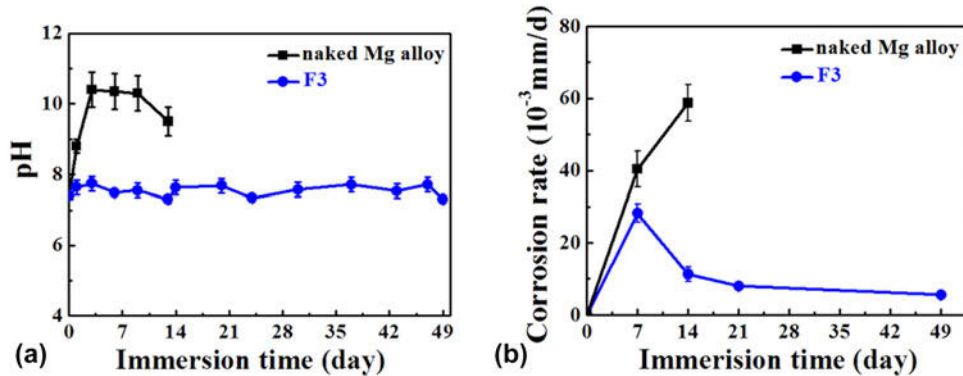| Samples	R_s (Ω cm^2)	R_1 (kΩ cm^2)	Q_1 μS/(cm^2 s)	n_1	R_2 (kΩ cm^2)	Q_2 μS/(cm^2 s)	n_2
F1	$10^{-7} \pm 10^{-10}$	165.00 ± 12.54	11.00 ± 4.40	0.70 ± 0.02	3.00 ± 0.2	0.16 ± 0.012	0.80 ± 0.04
F2	$2.00 \times 10^{-7} \pm 8.00 \times 10^{-10}$	200.00 ± 15.90	9.73 ± 3.40	0.69 ± 0.02	4.00 ± 0.26	9.24 ± 0.56	0.84 ± 0.03
F3	$10^{-7} \pm 4.00 \times 10^{-10}$	312.00 ± 12.69	8.00 ± 0.22	0.80 ± 0.02	16.00 ± 1.60	3.38 ± 0.51	0.48 ± 0.02

FIG. 4. (a) pH variation of the SBF and (b) corrosion rates of F3 and naked magnesium alloy after immersion in SBF for different periods.
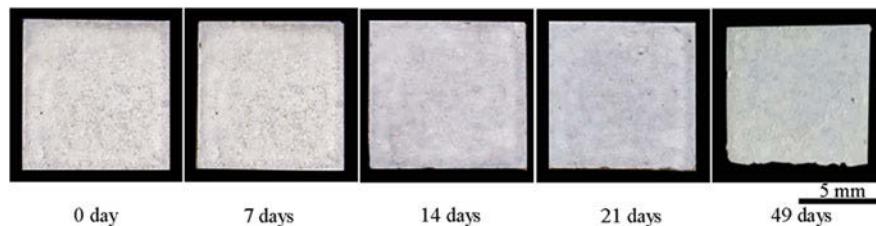

FIG. 5. Macroscopic appearances of F3 and naked magnesium alloy after immersion in SBF for different periods.

[Fig. 4(b)]. After 7 days of immersion, the corrosion rate of F3 is 28.20×10^{-3} mm/d. After 14 days of immersion, the corrosion rate of F3 kept stable as 11.30×10^{-3} mm/d, while the naked magnesium alloy presented serious corrosion with a corrosion rate of 58.70×10^{-3} mm/d.[15] With immersion time further prolonging, the corrosion rate of F3 presented a declining tendency (the corrosion rate at 49 days of immersion was 5.60×10^{-3} mm/d). Moreover, after 49 days of immersion, F3 still remained the original macroscopic appearance (Fig. 5). The results of SBF pH value variation, corrosion rate, and macroscopic appearance of F3 demonstrated that this composite coating could provide effective long-term protection for magnesium alloys in SBF.

The structure of the original protective coating and formed mineralized layer had an important impact on the long-time protection for magnesium alloys. To investigate the protective mechanism of this fluoridated Ca–Mg–P composite coating, the surface and cross-sectional morphology of F3 after immersion in SBF for different times and the corresponding electrochemical properties were characterized.

Surface and cross-sectional morphology of F3 after immersion in SBF for different times are shown in Fig. 6 and Fig. 7. Since SBF is supersaturated with respect to apatite, after immersion for 7 days, some granular precipitates were formed on the surface of F3 [Fig. 6(a)], meaning relatively high bioactivity. Meanwhile, some microcracks occurred, which might be attributed to the partial dissolution of the Mg(OH)$_2$ matrix of the composite coating [Fig. 7(b)]. After immersion for 14 days, the surface of F3 became rougher [Fig. 6(b)]. Viewing in Fig. 7(c), the mineralized layer composed of granular precipitates became denser. Moreover, there formed many dendrites on the surface of the mineralized layer. After immersion for 21 days, the mineralized layer became uniform [Fig. 6(c)]. On the surface of the previously formed dendrite layer, a new mineralized layer was formed [Fig. 7(d)], which was similar to that after 7 days of immersion. After immersion for 49 days, the mineralized layer totally covered the original composite coating and became much rougher, accompanying disappearance of the microcracks. Based on the surface morphology evolution of the mineralized layer, it is

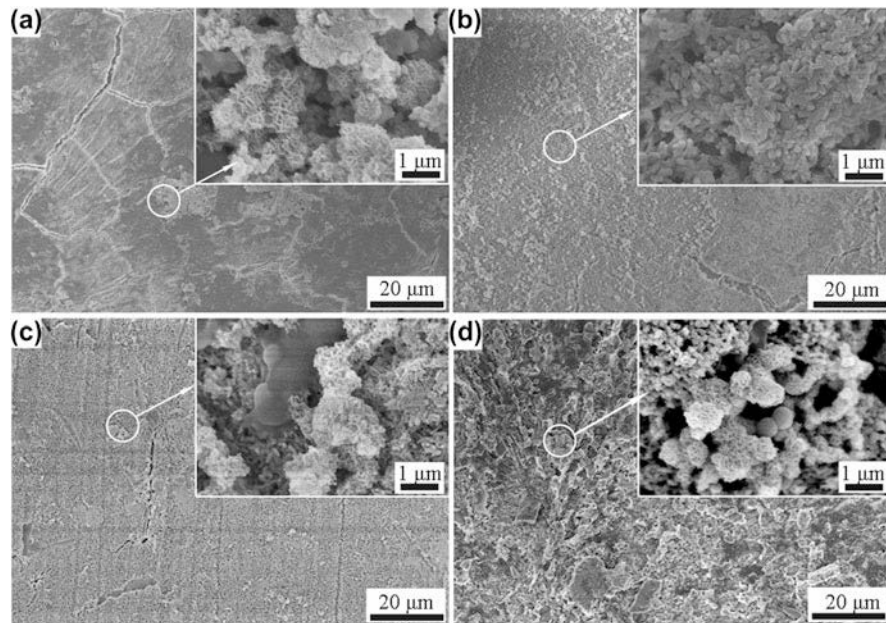J. Mater. Res., Vol. 33, No. 22, Nov 28, 2018

3797

FIG. 6. Surface morphologies of F3 after immersion in SBF for different periods: (a) 7 days, (b) 14 days, (c) 21 days, and (d) 49 days. The insets are the corresponding enlarged images.
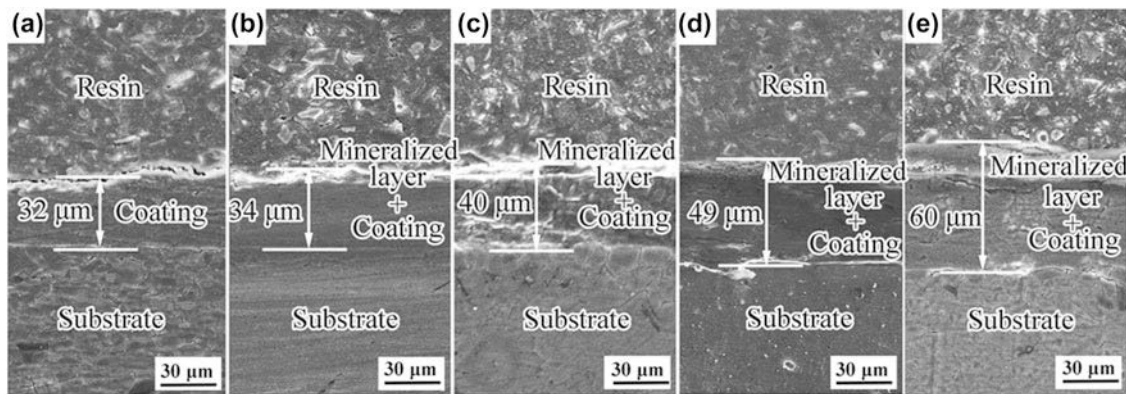

FIG. 7. Cross-sectional morphologies of F3 after immersion in SBF for different periods: (a) 0 day, (b) 7 days, (c) 14 days, (d) 21 days, and (e) 49 days.

reasonable to think that with immersion time prolonging, the mineralized layer was formed layer by layer. The previously formed mineralized layer was gradually densified to form dendrites. Simultaneously, the newly formed mineralized layer constantly precipitated. After immersion for 49 days, the mineralized layer and original composite coatings were integrated and their thickness reached 60 μm [Fig. 7(e)].

Correspondingly, the EIS test of F3 after immersion in SBF for different times was examined and is shown in Fig. 8. Generally, in the whole immersion time, R_t of F3 remained more than 100 kΩ cm^2. After 14 days of immersion, R_t of F3 exhibited an increase to 740 kΩ cm^2, which was mainly due to the densification of
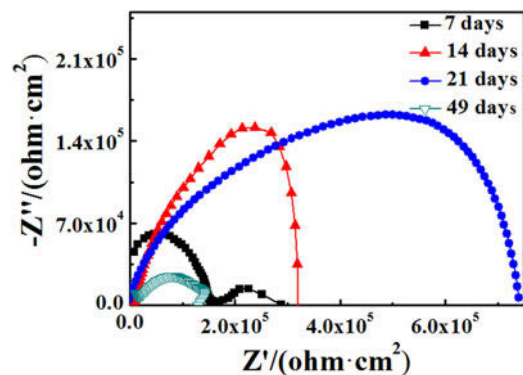

FIG. 8. Nyquist plots of F3 after immersion in SBF for different periods from 7 days to 49 days.

the formed mineralized layer. Specifically, with immersion time prolonging, there was not a recession for R_t of F3 compared with that of F3 before immersion, meaning that this fluoridated Ca–Mg–P composite coating and the formed mineralized layer were enough dense and possessed proper thickness to retard the penetration of SBF, thus acting as a physical barrier to provide effective protection for the magnesium alloy as long as 49 days.

IV. CONCLUSION

In this work, fluoridated Ca–Mg–P composite coatings were fabricated on magnesium alloys via a hydrothermal-assisted sol–gel process. With the increase of fluorine doping content from F1 to F3, $Mg(OH)_2$ content in the composite coatings increased and the surface structure tended to be dense, thus improving the corrosion resistance of the sample. F3 showed high charge transfer resistance of approximately 312 kΩ cm^2. Moreover, this composite coating quickly induced mineralized layer formation, which was gradually densified and integrated with the original composite coating. After immersion in SBF for 49 days, the coating thickness reached 60 μm. It is the dense and dissolution-resistant fluoridated Ca–Mg–P composite coating with large thickness and formed mineralized layer that provides effective long-term protection for magnesium alloys. Therefore, this fluoridated Ca–Mg–P composite coating could act as a promising protective coating on magnesium and magnesium alloy implants for orthopedic applications.

REFERENCES

1. M. Esmaily, J.E. Svensson, S. Fajardo, N. Birbilis, G.S. Frankel, S. Virtanen, R. Arrabal, S. Thomas, and L.G. Johansson: Fundamentals and advances in magnesium alloy corrosion. *Prog. Mater. Sci.* **89**, 92–193 (2017).
2. S.V. Dorozhkin: Calcium orthophosphate coatings on magnesium and its biodegradable alloys. *Acta Biomater.* **10**, 2919–2934 (2014).
3. Y. Xiong, X. Hu, and R. Song: Characteristics of CeO₂/ZrO₂-HA composite coating on ZK60 magnesium alloy. *J. Mater. Res.* **32**, 1073–1082 (2017).
4. S. Fooladi and S.R. Kiahosseini: Creation and investigation of chitin/HA double-layer coatings on AZ91 magnesium alloy by dipping method. *J. Mater. Res.* **32**, 2532–2541 (2017).
5. T.S. Lim, H.S. Ryu, and S.H. Hong: Plasma electrolytic oxidation/cerium conversion composite coatings for the improved corrosion protection of AZ31 Mg alloys. *J. Electrochem. Soc.* **160**, 73–82 (2013).
6. J. Qi, T. Hashimoto, J. Walton, X. Zhou, P. Skeldon, and G.E. Thompson: formation of a trivalent chromium conversion coating on AA2024-t351 alloy. *J. Electrochem. Soc.* **163**, 25–35 (2016).
7. S. Bauer, P. Schmuki, K. von der Mark, and J. Park: Engineering biocompatible implant surfaces part I: Materials and surfaces. *Prog. Mater. Sci.* **58**, 261–326 (2013).
8. K. Gregorczyk, and M. Knez: Hybrid nanomaterials through molecular and atomic layer deposition: Top down, bottom up, and in-between approaches to new materials. *Prog. Mater. Sci.* **75**, 1–37 (2016).
9. L. Chang, F. Cao, J. Cai, W. Liu, J. Zhang, and C. Cao: Formation and transformation of $Mg(OH)_2$ in anodic coating using FTIR mapping. *Electrochem. Commun.* **11**, 2245–2248 (2009).
10. Y.J. Shi, J. Pei, J. Zhang, J.L. Niu, H. Zhang, S.R. Guo, Z.H. Li, and G.Y. Yuan: Enhanced corrosion resistance and cytocompatibility of biodegradable Mg alloys by introduction of $Mg(OH)_2$ particles into poly(L-lactic acid) coating. *Sci. Rep.* **7**, 1–10 (2017).
11. H. Tang, F.J. Xu, W. Tao, and X. Jian: Fabrication and characterization of $Mg(OH)_2$ films on AZ31 magnesium alloy by alkali treatment. *Int. J. Electrochem. Sci.*, **12**, 1377–1388 (2017).
12. J. Jayaraj, S. Amruth Raj, A. Srinivasan, S. Ananthakumar, U.T.S. Pillai, N.G.K. Dhaipule, and U.K. Mudali: Composite magnesium phosphate coatings for improved corrosion resistance of magnesium AZ31 alloy. *Corros. Sci.* **113**, 104–115 (2016).
13. Q. Zhao, W. Mahmood, and Y. Zhu: Synthesis of dittmarite/Mg(OH)₂ composite coating on AZ31 using hydrothermal treatment. *Appl. Surf. Sci.* **367**, 249–258 (2016).
14. T. Ishizaki, R. Kudo, T. Omi, K. Teshima, T. Sonoda, I. Shigematsu, and M. Sakamoto: Corrosion resistance of multi-layered magnesium phosphate/magnesium hydroxide film formed on magnesium alloy using steam-curing assisted chemical conversion method. *Electrochim. Acta* **62**, 19–29 (2012).
15. S. Shen, S. Cai, Y. Li, R. Ling, F. Zhang, G. Xu, and F. Wang: Microwave aqueous synthesis of hydroxyapatite bilayer coating on magnesium alloy for orthopedic application. *Chem. Eng. J.* **309**, 278–287 (2017).
16. M. Manso, J.M. Martínez-Duart, M. Langlet, C. Jiménez, P. Herrero, and E. Millon: Aerosol–gel-derived microcrystalline hydroxyapatite coatings. *J. Mater. Res.* **17**, 1482–1489 (2011).
17. N. Yu, S. Cai, F. Wang, F. Zhang, R. Ling, Y. Li, Y. Jiang, and G. Xu: Microwave assisted deposition of strontium doped hydroxyapatite coating on AZ31 magnesium alloy with enhanced mineralization ability and corrosion resistance. *Ceram. Int.* **43**, 2495–2503 (2017).
18. S-H. Wang, C-W. Yang, and T-M. Lee: Evaluation of microstructural features and in vitro biocompatibility of hydrothermally coated fluorohydroxyapatite on AZ80 Mg alloy. *Ind. Eng. Chem. Res.* **55**, 5207–5215 (2016).
19. Y. Wang, S. Zhang, X. Zeng, L.L. Ma, W. Weng, W. Yan, and M. Qian: Osteoblastic cell response on fluoridated hydroxyapatite coatings. *Acta Biomater.* **3**, 191–197 (2007).
20. F.C.M. Driessens: Relation between apatite solubility and anti-cariogenic effect of fluoride. *Nature* **243**, 420–421 (1973).

21. L. Zhang, J. Pei, H. Wang, Y. Shi, J. Niu, F. Yuan, H. Huang, H. Zhang, and G. Yuan: Facile preparation of poly(lactic acid)/brushite bilayer coating on biodegradable magnesium alloys with multiple functionalities for orthopedic application. *ACS Appl. Mater. Interfaces* **9**, 9437–9448 (2017).

22. D.C. Romonţi, J. Iskra, M. Bele, I. Demetrescu, and I. Milošev: Elaboration and characterization of fluorohydroxyapatite and fluoroapatite sol–gel coatings on CoCrMo alloy. *J. Alloys Compd.* **665**, 355–364 (2016).

23. L. Gan and R. Pilliar: Calcium phosphate sol–gel-derived thin films on porous-surfaced implants for enhanced osteoconductivity. Part I: Synthesis and characterization. *Biomaterials* **25**, 5303–5312 (2004).

24. J. Zeng, C. Lin, J. Li, and K. Li: Low temperature preparation of barium titanate thin films by a novel sol–gel-hydrothermal method. *Mater. Lett.* **38**, 112–115 (1999).

25. N. Lu, Y. Zhao, H. Liu, Y. Guo, X. Yuan, H. Xu, H. Peng, and H. Qin: Design of polyoxometallate–titania composite film ($H_3PW_{12}O_{40}/TiO_2$) for the degradation of an aqueous dye Rhodamine B under the simulated sunlight irradiation. *J. Hazard. Mater.* **199–200**, 1–8 (2012).

26. H. Duan, Y.F. Zheng, Y.Z. Dong, X.G. Zhang, and Y.F. Sun: Pyrite (FeS_2) films prepared via sol–gel hydrothermal method combined with electrophoretic deposition (EPD). *Mater. Res. Bull.* **39**, 1861–1868 (2004).

27. X. Zhang, S. Böhm, A.J. Bosch, E.P.M. van Westing, and J.H.W. de Wit: Influence of drying temperature on the corrosion performance of chromate coatings on galvanized steel. *Mater. Corros.* **55**, 501–510 (2004).

28. W. Lv, X. Lv, J. Xiang, Y. Zhang, S. Li, C. Bai, B. Song, and K. Han: A novel process to prepare high-titanium slag by carbothermic reduction of pre-oxidized ilmenite concentrate with the addition of Na_2SO_4. *Int. J. Miner. Process.* **167**, 68–78 (2017).

29. R.M. Bandeira, J. van Drunen, A.C. Garcia, and G. Tremiliosi-Filho: Influence of the thickness and roughness of polyaniline coatings on corrosion protection of AA7075 aluminum alloy. *Electrochim. Acta* **240**, 215–224 (2017).

30. K.S. Le Corre, E. Valsami-Jones, P. Hobbs, and S.A. Parsons: Impact of calcium on struvite crystal size, shape and purity. *J. Cryst. Growth* **283**, 514–522 (2005).

31. R. Manoj Kumar, K.K. Kuntal, S. Singh, P. Gupta, B. Bhushan, P. Gopinath, and D. Lahiri: Electrophoretic deposition of hydroxyapatite coating on Mg–3Zn alloy for orthopaedic application. *Surf. Coat. Technol.* **287**, 82–92 (2016).

32. H. Tang, T. Wu, and W. Hong: Corrosion behavior of the HA containing ceramic coated magnesium alloy in Hank's solution. *J. Alloys Compd.* **698**, 643–653 (2017).

33. L. Abdoli, J. Huang, and H. Li: Electrochemical corrosion behaviors of aluminum-based marine coatings in the presence of *Escherichia coli* bacterial biofilm. *Mater. Chem. Phys.* **173**, 62–69 (2016).

34. V. Shinde and P.P. Patil: Evaluation of corrosion protection performance of poly(o-ethyl aniline) coated copper by electrochemical impedance spectroscopy. *Mater. Sci. Eng., B* **168**, 142–150 (2010).

35. G. Liu, S. Tang, D. Li, and J. Hu: Self-adjustment of calcium phosphate coating on micro-arc oxidized magnesium and its influence on the corrosion behaviour in simulated body fluids. *Corros. Sci.* **79**, 206–214 (2014).

Supplementary Material

To view supplementary material for this article, please visit https://doi.org/10.1557/jmr.2018.270.